11-7-2019

Charging and supercharging of proteins for mass spectrometry: recent insights into the mechanisms of electrospray ionization.

Lars Konermann

Haidy Metwally

Quentin Duez

Insa Peters

Invited 'Critical Review' for *Analyst*

Charging and Supercharging of Proteins for Mass Spectrometry: Recent Insights into the Mechanisms of Electrospray Ionization

Lars Konermann*, Haidy Metwally, Quentin Duez, and Insa Peters

Department of Chemistry, The University of Western Ontario, London, Ontario, N6A 5B7, Canada

* corresponding author: konerman@uwo.ca

Running Title: Mechanisms of Protein ESI

Abstract

Electrospray ionization (ESI) is an essential technique for transferring proteins from solution into the gas phase for mass spectrometry and ion mobility spectrometry. The mechanisms whereby $[M + zH]^{z+}$ protein ions are released from charged nanodroplets during ESI have been controversial for many years. Here we discuss recent computational and experimental studies that have shed light on many of the mysteries in this area. Four types of protein ESI experiments can be distinguished, each of which appears to be associated with a specific mechanism. (i) Native ESI proceeds according to the charged residue model (CRM) that entails droplet evaporation to dryness, generating compact protein ions in low charge states. (ii) Native ESI supercharging is also a CRM process, but the dried-out proteins accumulate additional charge because supercharging agents such as sulfolane interfere with the ejection of small ions (Na^+, NH_4^+, etc.) from the shrinking droplets. (iii) Denaturing ESI follows the chain ejection model (CEM), where protein ions are gradually expelled from the droplet surface. H^+ equilibration between the droplets and the protruding chains culminates in highly charged gaseous proteins, analogously to the collision-induced dissociation of multi-protein complexes. (iv) Denatured ESI supercharging also generates protein ions via the CEM. Supercharging agents stabilize protonated sites on the protein tail via charge-dipole interactions, causing the chain to acquire additional charge. There will likely be scenarios that fall outside of these four models, but it appears that the framework outlined here covers most of the experimentally relevant conditions.

1. Introduction - A Renaissance in ESI Mechanistic Research

The capability to transfer proteins and other biological macromolecules from solution into the gas phase by electrospray ionization (ESI) has revolutionized mass spectrometry (MS). ESI[1] and nanoESI[2, 3] continue to open up new avenues, from fundamental biophysics to applications in the biopharmaceutical industry.[4, 5] Major progress has been made in deciphering the mechanisms of ESI since we last reviewed this field in 2013.[6] Here we summarize these advances, with emphasis on proteins.

When writing this review, we assumed that readers will be familiar with some basic concepts that include the following:[6, 7] The ESI source represents an electrochemical cell that disperses analyte solution into a mist of charged droplets.[8] The droplets shrink due to evaporation and jet fission, ultimately resulting in nanodroplets that release analyte ions into the gas phase.[9] A differentially pumped interface transmits these ions into the vacuum of the mass spectrometer.[10, 11] ESI can be performed in positive or negative polarity. We will restrict our discussion to the positive ion mode which is most commonly used for proteins, generating multiply protonated $[M + zH]^{z+}$ ions.[6, 7] "Native" ESI experiments aim to preserve protein structures and interactions in the gas phase; these studies employ aqueous solutions at near-neutral pH, along with gentle declustering conditions during ion sampling.[12-25] On the other hand, "denaturing" ESI typically involves the use of acidified aqueous/organic mixtures that cause protein unfolding, along with the disruption of protein-ligand and protein-protein contacts.[26-28]

The mechanisms whereby gaseous proteins are released from ESI nanodroplets continue to be controversial. Experimental investigations in this area are challenging because of the short lifetimes, the small size, and the heterogeneity of droplets in the ESI plume. Many readers will recall the ESI-related battles that raged at conferences and in the literature during the 1990s. Those disputes were dominated by two competing ideas, Dole's charged residue model (CRM)[29] and the

ion evaporation model (IEM) of Iribarne and Thomson.[30] During the early 2000s the field calmed down, as members of both camps agreed to disagree or (perhaps) moved on to greener pastures.

The past few years have witnessed a renaissance in ESI mechanistic research that has been fueled by several factors: (1) Native ESI practitioners continue to expand the size and complexity of biomolecular assemblies that are being subjected to gas phase investigations,[16-25, 31] reviving the debate to what extent gaseous macroions retain solution-like conformations.[32-38] (2) Interest in the properties of gas phase proteins has intensified after the introduction of commercial ion mobility spectrometry (IMS) instruments that are now used in numerous laboratories for probing the conformations of biomolecular ions.[39-42] (3) Supercharging agents (SCAs) such as sulfolane, *m*-nitrobenzyl alcohol (*m*-NBA), or propylene carbonate have opened up novel ways to modulate protein charge states, thereby challenging existing ESI models.[43-45] (4) An expanding arsenal of dissociation techniques has opened the door to top-down methodologies that complement traditional bottom-up workflows.[33, 46-52] Top-down fragmentation efficiencies are closely related to protein charge states, highlighting the need to understand analyte charging mechanisms. (5) Many groups have begun to take advantage of breakthroughs in computer software and hardware for exploring ESI mechanistic aspects using molecular dynamics (MD) simulations.[53-65]

The following sections summarize current views of how gaseous protein ions are generated during ESI, how the ESI mechanism dictates charge states and gas phase conformations, and how these factors can be modulated by experimental parameters. Much of this discussion will revolve around recent MD data. Technical "how to" aspects of these computational endeavors have been reviewed elsewhere.[63] The considerations below apply to both ESI and nanoESI, because the final steps of gas phase ion formation are believed to be the same in both cases.[7] NanoESI can provide improved desolvation, greater salt tolerance, and a higher ion yield. [66-69] These aspects are believed to reflect the smaller initial droplet size in nanoESI,[2] which results from the smaller emitter tip

diameter and the lower solution flow rate. Prior to commencing our review of protein behavior during ESI, it is helpful to consider a few general aspects related to ESI droplets.

2. ESI Droplets: Solvents, Charge, and Stability

Late ESI droplets that release analyte ions into the gas phase have radii of a few nanometers.[7] These nanodroplets are formed by jet fission and evaporation from larger droplets that emanate from a Taylor cone at the ESI emitter tip.[6, 7, 70, 71] Our primary interest is in *water* droplets. The reason for this selection is obvious in the case of native ESI, which always employs aqueous solutions. In contrast, denaturing ESI usually involves acidified mixtures of water and methanol or acetonitrile. However, these water/organic mixtures undergo differential evaporation. The organic component has a higher vapor pressure, causing late ESI nanodroplets to be mostly aqueous[72-75] (ESI supercharging is an exception, see below).

Much of the droplet charge is attributable to small cations such as H^+, Na^+, and NH_4^+ which are present in excess compared to their counterions. Protons may originate from acids added to the solution, or from water electrolysis at the metal/liquid interface of the ESI emitter.[7, 8] Na^+ and other metal ions are ubiquitous in biological samples; their presence is apparent from metal adducts on electrosprayed protein ions.[76] These adducts tend to degrade the spectral quality, as they split the signal intensity of any protein charge state z into various peaks. Counterions such as Cl^- may participate in adduct formation as well, giving rise to heterogeneous $[M + (z\text{-}n\text{+}m)H + nNa + mCl]^{z+}$ ion populations where n and m adopt a range of different values. Various desalting strategies have been developed to mitigate the detrimental effects of nonvolatile salts, and to promote the formation of clean $[M + zH]^{z+}$ ions.[77, 78]

NH_4^+ in ESI droplets stems from ammonium acetate which is a standard solution additive in native ESI-MS.[7] Ammonium acetate allows native ESI experiments to be conducted in the presence of a background electrolyte that, to some extent, mimics a physiological environment.[79] Although ammonium acetate in water produces pH 7, it has almost no buffering capacity at neutral pH. Thus, the widespread habit of calling ammonium acetate a "buffer" is quite misleading.[80] Ammonium acetate is ESI-compatible due to its volatility, *i.e.*, it evaporates during the final ESI stages without forming protein adducts (NH_4^+ $CH_3COO^- \rightarrow NH_3(g) + CH_3COOH(g)$). Similarly, NH_4^+ ions that initially bind to the surface of nascent protein ions will leave as $NH_3(g)$ during ion sampling, leaving behind a proton.

The net number of charges on an ESI droplet is referred to as z_D. It reflects the contributions from *all* charges, including dissolved ions as well as the protein charge which can be significant under conditions where pH ≠ pI . In his seminal 1882 paper[81] Rayleigh predicted that z_D on a spherical droplet cannot exceed the so-called Rayleigh limit z_R, defined as

$$z_R = 8\pi/e \times (\varepsilon_0 \gamma r^3)^{1/2} \qquad (1)$$

In this expression γ is the surface tension, r is the droplet radius, ε_0 is the vacuum permittivity, and e is the elementary charge.[7] For many applications it is convenient to report droplet charge as the ratio z_D/z_R. The Rayleigh limit corresponds to $z_D/z_R = 1$. For $z_D/z_R << 1$ the droplet is stable, because cohesive forces among the solvent molecules dominate over Coulombic repulsion. As z_D/z_R approaches unity, the electrostatically stressed droplet becomes unstable, thereby trigging jet fission or other charge loss events. Experiments have confirmed that ESI droplets occupy a z_D/z_R regime between 0.7 and 1.[7, 70, 73]

3. Charge Loss from Nanodroplets at the Rayleigh Limit – the Ion Evaporation Model (IEM)

MD simulations on ESI droplets that contain H^+ or NH_4^+ face significant computational challenges.[63] Such studies are only meaningful if they account for Grotthus shuttling, i.e., rapid proton transfer along "water wires", a feature that is not included in classical MD force fields.[82-84] The situation is much more straightforward for metal cations such as Na^+. For this reason, most of the concepts discussed here will be illustrated with Na^+-charged aqueous nanodroplets. MD data that illustrate the behavior of such droplets are depicted in Figure 1. The simulated trajectories exhibit multiple IEM events, where small $[H_2O_n + Na]^+$ clusters with $n \approx 10$ are ejected from the droplet surface (Figure 1A). Another example is the IEM ejection of Na^+/crown ether complexes (Figure 1B), a process that is relevant for recent mechanistic investigations.[85-88] All these IEM events are driven by the electric field that emanates from the highly charged droplet.[6, 30] IEM ejection requires crossing of a free energy barrier that arises from the combination of Coulombic repulsion with attractive interactions caused by the polarization of water dipoles.[53, 89]

In addition to the typical IEM ejection events of Figure 1A, Na^+-charged droplets occasionally eject larger moieties, e.g., one Na^+ with ~40 water molecules (Figure 1C) or two Na^+ and ~120 waters (Figure 1D). It is tempting to interpret these departing assemblies as small offspring droplets, a view that is supported by the resemblance of Figure 1C/D with fission events that have been documented in imaging experiments on larger droplets.[70, 90] Hence, it may not be possible to draw a clear line between IEM ejection and droplet fission,[6] although the older literature suggests that these two processes are completely distinct from one another.[7, 30] In any case, the MD snapshots of Figure 1A-D demonstrate that highly charged nanodroplets undergo

charge loss events that can follow different morphologies, with the classical IEM being most prevalent (Figure 1A). [30, 89]

Figure 1E provides a closer look at the temporal evolution of a charged nanodroplet. Water evaporation causes rapid droplet shrinkage, accompanied by numerous IEM events that decrease the number of Na^+ in a stepwise fashion. A plot of z_D/z_R reveals a saw tooth pattern (Figure 1F). Sudden downward transitions in this graph reflect IEM events that reduce the Coulombic repulsion within the droplet. Each of these events is followed by solvent evaporation at constant z_D. These evaporation phases gradually build up electrostatic stress by confining the droplet charge to a steadily shrinking volume, until the system becomes unstable and the next IEM event takes place. All charge loss events in Figures 1F occur at (or slightly below) the Rayleigh limit, consistent with theoretical predictions[81] and experimental observations.[7, 70, 73] Hence, MD simulations of the type depicted in Figure 1 describe the nanodroplet behavior remarkably well. IEM events similar to those illustrated here for Na^+ are believed to take place for other ESI-relevant charge carriers, such as H^+ or NH_4^+.[6, 91, 92]

Although typical ESI droplets contain abundant cations that are conducive to IEM events,[7] it is interesting to speculate what would happen for pure aqueous solution. Specifically, let's consider a droplet consisting of pure water that contains a highly positively charged protein. Would solvent evaporation in this hypothetical scenario take place without IEM events, producing droplets that exceed the Rayleigh limit ($z_D/z_R >> 1$)? We believe this to be unlikely. IEM events would still take place, because ejectable H^+ would be available from the dissociation of basic side chains (e.g. $Lys^+ \leftrightarrow Lys + H^+$) and from the self-ionization of water ($H_2O \leftrightarrow OH^- + H^+$). Standard MD force fields are unsuitable for modeling these phenomena,[53-55, 57-63] calling for future *ab-initio* investigations.[93-95] Experiments indicate that there can be situations where droplets slightly exceed the Rayleigh limit (e.g. $z_D/z_R \approx 1.4$),[73] but there is no experimental evidence for scenarios with

$z_D/z_R >> 1$. Thus, the IEM represents an unavoidable "electrostatic stress relief valve" that keeps ESI droplets close to the Rayleigh limit.

4. A Few Words about Myoglobin

Myoglobin (Mb) has been used as model protein in numerous ESI mechanistic investigations.[13, 26, 96-100] Native holo-Mb in solution is folded into a compact helical structure, with a hydrophobic core and a hydrophilic/charged exterior.[101] The native protein contains a weakly bound heme group, making it an ideal test system for probing the behavior of noncovalent protein-ligand complexes. The native state is stable at pH 7, while acidification yields heme-free apo-Mb that is extensively unfolded.[102]

The use Mb as a model system is not limited to MS-related research. Instead, its reputation as one of the most "ordinary" proteins has made it a de-facto paradigm for a wide range of biophysical studies.[103-106] Many of those investigations implicitly assume that fundamental insights obtained for Mb will also apply to most other proteins. Analogously, we believe that the ESI principles discussed below for Mb are quite general.

5. Four Types of Experimental ESI Conditions

Four main ESI conditions can be distinguished. They reflect the different solution environments experienced by proteins within the electrospray capillary or the nanoESI emitter (Figure 2). We distinguish native and denaturing ESI, each of which can be performed under "regular" conditions or in the presence of a supercharging agent. The four conditions produce $[M + zH]^{z+}$ ions with

dramatically different charge states. (i) *Native ESI* employs non-denaturing aqueous solutions at near-neutral pH, generating holo-Mb ions in very low charge states (around 9+, Figure 2A). (ii) Almost the same conditions are used for *native supercharging ESI*, except that the solution is supplemented with a SCA such as sulfolane. Native supercharging produces holo-Mb ions in elevated charge states, with a maximum at 16+ (Figure 2B). (iii) *Denaturing ESI* is implemented by electrospraying proteins that are unfolded in bulk solution. This is illustrated in Figure 2C for acid-unfolded apo-Mb, producing a charge state distribution that peaks at 23+. (iv) *Denatured Supercharging ESI* employs solution-phase unfolding in the presence of a SCA. Apo-Mb ions produced in this way have a charge state distribution that peaks at 27+ and extends to 33+ (Figure 2D). The 33+ charge state coincides with the theoretical maximum z value for apo-Mb, assuming that every titratable site is protonated (N-terminus$^+$, Arg$^+$, Lys$^+$, His$^+$, Glu^0, Asp^0, C-terminus^0).[107] Denatured supercharging can sometimes even produce charge states that exceed this expected maximum, indicating that additional sites can participate in protonation.[108, 109]

As a word of caution, it has occasionally been suggested that the charge states seen under the various conditions of Figure 2 mirror the titration behavior of the protein in bulk solution. Experiments have debunked this myth many years ago, demonstrating that protein charge states in solution and after ESI are unrelated.[6, 110-112] Instead, the number of charges that is bound to an electrosprayed protein depends on the mechanism by which the analyte is transferred from the droplet into the gas phase, as outlined in the subsequent sections.

6. MD Simulations of the ESI Process

All MD data discussed below were initiated using nanodroplets that were charged close to the Rayleigh limit. Each droplet contained a single protein. X-ray coordinates of holo-Mb served as

starting point for native ESI simulations, with an initial droplet radius of 4 nm. All titratable sites for these native ESI runs were in their default protonation states (N-terminus$^+$, Arg$^+$, Lys$^+$, His^0, Glu$^-$, Asp$^-$, C-terminus$^-$).[85, 113, 114] Acid-unfolded apo-Mb was used in the case of denaturing ESI, employing a larger droplet radius of 5.5 nm to ensure that the chains were fully contained within the droplets at the onset of the runs. To mimic their acidic environment the denatured chains were modeled as poly-cations that had Glu, Asp, and C-terminus in their neutral R-COOH forms.[107, 115] Readers interested in additional simulation details are encouraged to consult ref.[63]

In our simulations we strived to avoid any factors that would bias the simulations toward specific outcomes. In other words, it was *not* our aim to prove or disprove certain ESI models. Instead, we simply observed how the droplets evolved over time, while each atom followed its trajectory as governed by the laws of Physics.[63, 113] The following sub-sections highlight MD data that mimic the four experimental ESI conditions. Illustrative MD snapshots are shown in Figure 3A-D, and mechanistic details extracted from the simulations are summarized in the cartoons of Figure 2A-D.

6A. Native ESI: Charged Residue Model (CRM)

MD runs of native holo-Mb employed water droplets that were charged with Na^+, sidestepping challenges associated with H^+ or NH_4^+ simulations (Figure 3A).[63, 82-84] Water evaporation gradually reduced the droplet radius, with occasional IEM ejection of Na^+. Throughout this evaporation process the folded protein remained in the droplet interior, reflecting the tendency of charged/polar side chains on the protein surface to maximize solvation by the aqueous environment.[101] Evaporation of the final water layers eventually released the protein into the gas

phase (Figure 3A). This sequence of events, with analyte release via solvent evaporation to dryness represents the hallmark of the CRM.[6, 7, 29, 116, 117]

The IEM ejection of low MW charge carriers plays an ancillary role during the CRM, by ensuring that the shrinking droplets stay close to the Rayleigh limit (Figure 1F).[91, 92] Those charge carriers that are still present during the final stages of solvent evaporation associate with acidic side chains. For Na^+-containing droplets these conditions produced $[M + zNa]^{z+}$ ions (Figure 3A). Analogously, protein charging via NH_4^+ would generate $[M + zH]^{z+}$ ions, because NH_4^+ adducts are converted to H^+ due to NH_3 loss during ion sampling (see section 2).[6, 7, 114]

The fact that the shrinking droplets stay close to the Rayleigh limit implies that CRM-produced protein ions will end up with a charge state z that is close to z_R of a protein-sized water droplet.[7, 114, 116] For the simulations of Figure 3A these conditions yielded 9+ protein ions, consistent with experimental data of Figure 2A. Similar agreement between simulated and experimental charge states was also observed for ubiquitin and cytochrome *c*, and for MD runs covering a range of initial solution-phase charge values.[114]

Gaseous protein ions produced under simulation conditions similar to Figure 3A all retained solution-like conformations,[114] supporting the view that native ESI allows the retention of biologically relevant structures and interactions due to kinetic trapping.[118-120] Survival of these native-like elements is fostered by the fact that CRM charge states are low, such that Coulombically driven unfolding of the gaseous proteins is avoided (Figure 4A).[96, 119, 121-123]

In summary, the CRM represents the dominant mechanism by which globular proteins are transferred from solution into the gas phase during native ESI (see cartoon summary in Figure 2A). This view is supported by the MD data discussed here,[114, 124] and by numerous earlier studies.[6, 7, 43, 116, 117] CRM scenarios have also been proposed for other analytes, including nucleic acid duplexes,[59] peptides,[60, 61] and salt clusters.[67] Solvent evaporation to dryness implies that

contaminants in the analyte solution will tend to cause nonspecific adducts, providing a simple explanation for the vulnerability of the ESI process to nonvolatile salts.[7]

6B. Native Supercharging ESI: CRM with Charge Trapping

Background. The low protein charge states produced by native ESI can be disadvantageous under some conditions. For example, ions with low *z* tend to be unreactive in top-down experiments,[46, 125] and they are not well suited for Fourier transform mass analyses.[126, 127] One way to boost the protein charge is to use denaturing conditions, as discussed below. SCAs such as sulfolane ($C_4H_8SO_2$, Figure 2B) represent an alternative strategy to enhance the charge of protein ions.[43-45] In this section we focus on *native* supercharging,[99, 128-133] where proteins experience a non-denaturing solvent environment as they enter the ESI source.[91, 115-120] Native supercharging is illustrated in Figure 2A/B, where addition of 1% sulfolane to the neutral aqueous solution shifts the maximum of the experimental holo-Mb spectrum from 9+ to 16+.

SCAs share several characteristics. Their low volatility makes them evaporate slower than water, such that late ESI nanodroplets contain a much higher SCA percentage than the initial solution.[45, 98, 99, 134] They possess a greater dipole moment than water[45, 135, 136] (4.7 D for sulfolane vs. 1.85 D for H_2O),[107] their surface tension is between methanol and water,[45] and they exhibit low Brønsted basicity.[135] In the typically used concentration range (~1%) they do not affect the protein structure or stability in the bulk analyte solution.[99]

Earlier Supercharging Models. The mechanisms by which SCAs boost protein charge states in native ESI are controversial.[43, 98, 131, 134, 136, 137] Initial work focused on surface tension effects.[43] If the enrichment of SCAs during evaporation were to increase the surface tension, ESI droplets at

the Rayleigh limit should support more charge (Equation 1), thereby producing CRM ions with higher *z*. Unfortunately, this "surface tension model" cannot account for all the experimental observations.[72] For example, *m*-NBA enrichment in aqueous droplets *lowers* the surface tension ($\gamma_{m\text{-NBA}} < \gamma_{water}$), but *m*-NBA *increases* protein charging in native ESI.[98]

Another proposal attributes native ESI supercharging to thermal or chemical protein unfolding in the droplet.[99] This "unfolding model" has been disputed[44, 98, 124, 129, 138, 139] because the elevated collision cross sections observed for some supercharged proteins[97, 99, 124] do not prove that unfolding has taken place within the droplet. Just as likely, Coulombically-driven unfolding could occur after protein release into the gas phase.[124, 140] Many supercharged proteins retain their native ligands,[44, 98, 129] and some even preserve a native-like compactness.[129, 140] These observations make it unlikely that protein unfolding in the droplet constitutes the general root cause of native ESI supercharging.[44, 98, 124, 129, 138, 139]

The Charge Trapping Model. Simulations aimed at exploring the mechanism of native ESI supercharging were set up with holo-Mb in water/sulfolane droplets (Figure 3B).[85, 124] Evaporative droplet shrinkage was accompanied by the IEM ejection of Na^+. Water evaporated more quickly than sulfolane, reflecting the low vapor pressure of the SCA,[45, 98, 99, 134] and producing water-free protein/sulfolane droplets after ~90 ns. Na^+ binding to the protein followed by slow sulfolane evaporation ultimately yielded holo-Mb 16+. Gaseous protein ions in Figure 3B were released after solvent evaporation to dryness, i.e., native ESI supercharging represents a CRM process.[29]

It is remarkable that the MD data mirrored the experimentally observed shift, from 9+ in water to 16+ in water/sulfolane (Figure 2A/B). The reason behind this phenomenon can be uncovered by inspecting the MD trajectories.[85, 124] The key principle is simple: each Na^+ in the evaporating droplets can experience only two possible outcomes, IEM ejection or binding to the

protein. Thus, any suppression of IEM events will boost the protein charge. The MD data reveal that sulfolane disfavors IEM ejection in two ways (Figure 2B), both of which arise from the fact that Na^+ is highly soluble in water while having a low solubility in sulfolane.[124] (i) The droplets initially segregate into an outer sulfolane shell and an aqueous core. This core harbors protein and Na^+. The sulfolane shell restricts Na^+ access to the droplet surface, thereby impeding IEM ejection. (ii) Differential evaporation continuously drives up the sulfolane concentration, providing an increasingly poor Na^+ solvation environment. As the last water leaves, all the remaining Na^+ in the sulfolane droplet undergo irreversible binding to the protein (Figure 2B). This is in contrast to water droplets of the same size, where favorable solvation by H_2O ensures that Na^+ remain mobile, such that IEM events continue to occur (Figure 2A). In summary, the MD data suggest that a "charge trapping mechanism" is responsible for supercharging under native ESI conditions, a view that is consistent with earlier mechanistic proposals.[134, 135]

The discussion above focused on sulfolane, but virtually the same effects were observed for *m*-NBA,[124] suggesting that the mechanism is quite general. The charge trapping scenario demonstrated here for Na^+ also applies to NH_4^+ and other ESI-relevant charge carriers. Interestingly, crown ethers such as 18C6 suppress supercharging. This effect has been attributed to the fact that complexation by 18C6 solubilizes charge carriers in sulfolane, thereby preventing them from being trapped in the shrinking droplet.[85] The capability of 18C6 to act as supercharging antidote strongly supports the charge trapping model (Figure 2B).

Supercharged holo-Mb in our simulations underwent moderate Coulombic unfolding after attaining its final charge state, and after almost all the solvent had evaporated (bottom panels in Figures 2B, 3B).[85, 124] Thus, unfolding is a consequence of supercharging. This is in contrast to the aforementioned "unfolding model", where unraveling of the protein is considered to be the cause of supercharging.[99] The charge trapping model accounts for the experimental observation that

supercharging can take place even for proteins that retain a native-like structure in the gas phase.[129, 140] Nonetheless, we do not dispute that there may be some instances where unfolding in the droplet can contribute to the formation of high charge states.[99, 100, 141]

6C. Denaturing ESI: The Chain Ejection Model (CEM)

Denaturing ESI starts with unfolded proteins in solution, generating ions that carry more charge than after native or native/supercharging ESI (Figure 2C). Several years ago, we proposed that protein ions under denaturing ESI conditions form according to the chain ejection model (CEM, Figure 4A).[115] This model envisions that exposed hydrophobic residues cause the unfolded protein to migrate to the droplet surface. The chain is then gradually pushed out of the droplet, passing through intermediate structures where the droplet is decorated with a steadily growing protein tail. Ejection is driven by electrostatic repulsion between the droplet and the protein. The formation of high charge states is attributed to H^+ that migrate onto the extended tail, a process that results from the tendency of these charge carriers to maximize their spatial separation. Charge migration is facilitated by the high mobility of H^+ in water[82-84] and in gaseous proteins.[142-144] This charge migration continues until the protein detaches from the droplet.[115, 145, 146] The CEM is analogous to the collision-induced dissociation of multi-protein complexes. Both processes involve H^+ migration, followed by ejection of a highly charged chain (Figure 4B).[147-150] Related ESI extrusion scenarios have also been proposed for synthetic polymers,[151, 152] but those processes occur without H^+ migration which is a central element of the protein CEM.[6, 97, 145, 146]

Only very recently has it become possible to scrutinize the viability of protein CEM events in atomistic MD simulations with state-of-the-art force fields.[115] Data obtained in this way are illustrated in Figure 3C, depicting the behavior of acid-denatured apo-Mb in a Rayleigh-charged water droplet. Difficulties associated with H^+ migration between the droplet and the protein were

avoided in these simulations by focusing on specific pH values where gas phase and solution charge of the protein were close to one another.[115] The MD data support the view that unfolded protein chains get ejected from the droplet, in a manner that is consistent with our earlier CEM proposal (Figure 4A). Although the CEM was illustrated here for an acid-unfolded protein, it appears that the same mechanism applies to unfolded chains in general, including intrinsically disordered proteins (IDPs) that are electrosprayed from neutral aqueous solutions.[27, 37, 146]

The fact that denaturing ESI produces wide charge state distributions can be attributed to several factors. The ESI plume is heterogeneous and comprises droplets of different sizes.[7] Large droplets (that carry a larger absolute charge at the Rayleigh limit, see Equation 1) will impart more protons to a protein chain during ejection, while the opposite is true for smaller droplets.[6] In addition, not all proteins will be ejected from the droplet in exactly the same straight conformation. Instead, there will be instances where chains emerge in hairpin structures or as partially coiled conformers.[115] These conformational differences affect the number of H^+ imparted onto the protein; electrostatic calculations have revealed that perfectly straight chains tend to form the highest charge states, while protonation of less extended conformers will be less extensive.[6] In summary, the fact that denatured ESI conditions produce wide charge state distributions is attributed to a combination of droplet size effects and protein conformational factors. Despite the possible existence of slightly different conformations during ejection, the highly charged CEM ions tend to adopt near-linear stretched-out structures after separating from the droplet, as demonstrated in simulations and IMS experiments.[97, 115]

6D. Denatured Supercharging ESI: CEM with Charge Site Stabilization

The most highly charged protein ions are generated under conditions where denaturing ESI is conducted in the presence of a SCA (Figure 2D).[45, 97, 136, 153, 154] MD simulations of acid-unfolded apo-Mb in water/sulfolane droplets revealed that the ESI process under these conditions also follows the CEM (Figure 3D).[107] The events by which the protein chains got ejected from the ESI droplet were very similar to those discussed in the preceding section for sulfolane-free droplets (Figure 3C).

Close inspection of the simulation data reveals how the presence of SCAs boosts the protein charge under CEM conditions. The departing chain is heavily adducted with sulfolane (Figure 5). These adducts mainly interact with protonated basic sites on the protein, providing significant electrostatic stabilization of protein-bound H^+ via charge-dipole interactions. Readers are reminded that a central element of the CEM is the H^+ equilibration between the droplet and the protruding chain, driven by the electrostatic repulsion within the system (Figure 4A).[6] Sulfolane-mediated favorable charge-dipole interactions along the protein chain favor the accumulation of *additional* H^+ on the protein, thereby causing supercharging.

Two specific properties allow SCAs such as sulfolane to stabilize protonated sites on the protruding chain: (i) Their low vapor pressure makes them adhere to the protein chain that sticks out into the vapor phase.[45, 98, 99, 134] (ii) Their large dipole moment causes them to provide highly effective charge solvation.[45, 135, 136] Energetic analyses under the conditions of Figure 5B revealed that the presence of sulfolane provides an electrostatic stabilization of ~4000 kJ mol^{-1} compared to chains that emerged from water droplets (Figure 5A). This energy difference is roughly equivalent to four protonation events ($\Delta z \approx 4$) matching the experimental difference in spectral maxima, i.e., 23+ in water vs. 27+ in water/sulfolane (Figure 2C/D).[107]

Most SCA molecules that adhere to the nascent chains (Figure 2D, Figure 5B) are lost during ion activation in the sampling interface of the mass spectrometer. When minimizing in-

source activation it is possible to preserve some SCA adducts, but only on the most highly supercharged ions.[136] This adduction pattern is intriguing because nonspecific adducts typically affect low charge states to a greater extent, reflecting the fact that in-source activation is proportional to *z*.[21, 98, 155] The fact that SCA adducts are seen only for the most highly charged ions implies that SCA binding to the unfolded protein is directly involved in the formation of high charge states,[136] supporting the charge stabilization model of Figure 2D.[107] Similar to the CEM ions discussed above, apo-Mb electrosprayed under denatured supercharging conditions was found to adopt highly extended gas phase conformations.[97, 107]

In summary, SCAs boost protein charge states under both native and denaturing ESI conditions. The mechanistic foundation of this charge enhancement in the two cases, however, is very different. Native ESI supercharging takes place under CRM conditions, and enhanced protonation is attributed to charge trapping (Figure 2B).[85, 124] In contrast, denatured supercharging is a CEM process, and the shift to higher protonation states is caused by dipole-mediated stabilization of charge sites during chain ejection (Figure 2D).[107]

7. Conclusions

The ability to control the charge states of electrosprayed $[M + zH]^{z+}$ protein ions is essential for many applications because *z* governs the gas phase behavior of these analytes, including their conformations,[156, 157] transmission,[10] fragmentation,[125, 158] reactivity,[153, 154, 159] and detection.[126, 127] The most important determinant of protein charge states is the polypeptide conformation in solution and/or in the ESI droplets.[6, 26, 27, 100] Other factors can play a role as well, in particular, the presence or absence of SCAs affects the outcome of the ESI process.[43-45]

In this article we reviewed the current understanding of the protein ESI process, with focus on insights obtained from recent computational work. In Figure 2 we connected each of the four principal protein ESI modes with one specific mechanism. Native ESI was associated with the CRM, while native supercharging ESI was linked to a CRM/charge trapping scenario. Denaturing ESI is believed to proceed via the CEM. Denatured supercharging ESI was also identified as a CEM process, supplemented by dipole-mediated stabilization of protonated sites.

The compartmentalization of Figure 2 into four distinct pillars likely oversimplifies the situation to some extent. There may be conditions that fall in-between (or even outside) these proposed scenarios. For example, some proteins may exhibit CRM/CEM hybrid behavior, where chains undergo partial ejection but then experience solvent evaporation to dryness.[107, 146] Similarly, the native supercharging mechanism of Figure 2B envisions that proteins retain a compact structure until they have attained their final charge state; this does not exclude the possibility there could be instances where proteins unfold in the droplet.[99, 100, 141] Depending on the vapor environment experienced by the protein ions, it is possible that gas phase H^+ transfer might alter the charge states of protein ions after release from the droplet.[109] Lastly, the IEM was introduced in section 3 as a pathway for low MW charge carriers. It will be interesting to explore the upper size limit of the IEM, and to test whether some peptides or perhaps even small proteins can undergo IEM ejection under certain conditions.

The past five years have witnessed significant progress in the understanding of how analytes are transferred from solution into that gas phase during ESI. It is hoped that experiments and computational/theoretical endeavors will continue to provide new insights into this fascinating area.[160] Future studies should strive to understand the implications of mobile protons in solution (Grotthus shuttling)[82-84] and in the gas phase[142-144] for the ESI process, and they should include non-standard analytes such as IDPs[27, 37, 146] and large biomolecular complexes.[16-25]

Perhaps at some point the MS community should revisit the meaning of the third letter in the CRM, IEM, and CEM acronyms. At present, the "M" stands for "model". However, as evidence for the viability of these scenarios accumulates, the time may come to promote the "M" to "mechanism". The remaining challenge will then be to identify exactly under what experimental conditions each of the three models (mechanisms?) is operative.

Acknowledgements. Funding for this work was provided by the Natural Sciences and Engineering Research Council of Canada (NSERC, Grant Number RGPIN-2018-04243). Q.D. was supported by a FRS/FNRS Research Fellowship.

References

1. J. B. Fenn, *Angew. Chem. Int. Ed.*, 2003, **42**, 3871-3894.
2. M. Wilm and M. Mann, *Anal. Chem.*, 1996, **68**, 1-8.
3. G. T. T. Gibson, S. M. Mugo and R. D. Oleschuk, *Mass Spectrom. Rev.*, 2009, **28**, 918-936.
4. I. D. G. Campuzano and J. L. Lippens, *Curr. Op. Chem. Biol.*, 2018, **42**, 147-159.
5. G. B. Wang, P. V. Bondarenko and I. A. Kaltashov, *Analyst*, 2018, **143**, 670-677.
6. L. Konermann, E. Ahadi, A. D. Rodriguez and S. Vahidi, *Anal. Chem.*, 2013, **85**, 2-9.
7. P. Kebarle and U. H. Verkerk, *Mass Spectrom. Rev.*, 2009, **28**, 898-917.
8. G. J. Van Berkel and V. Kertesz, *Anal. Chem.*, 2007, **79**, 5511-5520.
9. N. B. Cech and C. G. Enke, *Mass Spectrom. Rev.*, 2001, **20**, 362-387.
10. T. R. Covey, B. A. Thomson and B. B. Schneider, *Mass Spectrom. Rev.*, 2009, **28**, 870-897.
11. V. Gabelica and E. De Pauw, *Mass Spectrom. Rev.*, 2005, **24**, 566-587.
12. B. Ganem, Y.-T. Li and J. D. Henion, *J. Am. Chem. Soc.*, 1991, **113**, 7818-7819.
13. V. Katta and B. T. Chait, *J. Am. Chem. Soc.*, 1991, **113**, 8534-8535.
14. J. A. Loo, *Int. J. Mass Spectrom.*, 2000, **200**, 175-186.
15. M. C. Fitzgerald, I. Chernushevich, K. G. Standing, C. P. Whitman and S. B. H. Kent, *Proc. Natl. Acad. Sci. U.S.A.*, 1996, **93**, 6851-6856.
16. A. C. Leney and A. J. R. Heck, *J. Am. Soc. Mass Spectrom.*, 2017, **28**, 5-13.
17. H. Zhang, W. D. Cui, M. L. Gross and R. E. Blankenship, *Febs Lett.*, 2013, **587**, 1012-1020.
18. A. Konijnenberg, A. Butterer and F. Sobott, *Biochim. Biophys. Acta*, 2013, **1834**, 1239-1256.
19. N. Khristenko, J. Amato, S. Livet, B. Pagano, A. Randazzo and V. Gabelica, *J. Am. Soc. Mass Spectrom.*, 2019, **30**, 1069-1081.
20. C. V. Robinson, *Proc. Natl. Acad. Sci. U. S. A.*, 2019, **116**, 2814-2820.
21. E. N. Kitova, A. El-Hawiet, P. D. Schnier and J. S. Klassen, *J. Am. Soc. Mass Spectrom.*, 2012, **23**, 431-441.
22. J. L. P. Benesch and B. T. Ruotolo, *Curr. Op. Struct. Biol.*, 2011, **21**, 641-649.
23. A. F. M. Gavriilidou, F. P. Holding, D. Mayer, J. E. Coyle, D. B. Veprintse and R. Zenobi, *Biochemistry*, 2018, **57**, 1685-1689.
24. O. Fatunmbi, R. R. Abzalimov, S. N. Savinov, A. Gershenson and I. A. Kaltashov, *Biochemistry*, 2016, **55**, 1918-1928.
25. G. T. H. Nguyen, T. N. Tran, M. N. Podgorski, S. G. Bell, C. T. Supuran and W. A. Donald, *ACS Centr. Sci.*, 2019, **5**, 308–318.
26. A. Dobo and I. A. Kaltashov, *Anal. Chem.*, 2001, **73**, 4763-4773.
27. J. Li, C. Santambrogio, S. Brocca, G. Rossetti, P. Carloni and R. Grandori, *Mass Spectrom. Rev.*, 2016, **35**, 111-122.
28. J. A. Loo, C. G. Edmonds, H. R. Udseh and R. D. Smith, *Anal. Chem.*, 1990, **62**, 693-698.
29. M. Dole, L. L. Mack, R. L. Hines, R. C. Mobley, L. D. Ferguson and M. B. Alice, *J. Chem. Phys.*, 1968, **49**, 2240-2249.
30. J. V. Iribarne and B. A. Thomson, *J. Chem. Phys.*, 1976, **64**, 2287-2294.
31. J. E. Keener, D. E. Zambrano, G. Z. Zhang, C. K. Zak, D. J. Reid, B. S. Deodhar, J. E. Pemberton, J. S. Prell and M. T. Marty, *J. Am. Chem. Soc.*, 2019, **141**, 1054-1061.

32. O. S. Skinner, F. W. McLafferty and K. Breuker, *J. Am. Soc. Mass Spectrom.*, 2012, **23**, 1011-1014.
33. T. Ly and R. R. Julian, *J. Am. Chem. Soc.*, 2010, **132**, 8602-8609.
34. E. R. Badman, C. S. Hoaglund-Hyzer and D. E. Clemmer, *Anal. Chem.*, 2001, **73**, 6000-6007.
35. C. Bich, S. Baer, M. C. Jecklin and R. Zenobi, *J. Am. Soc. Mass Spectrom.*, 2010, **21**, 286-289.
36. P. W. A. Devine, H. C. Fisher, A. N. Calabrese, F. Whelan, D. R. Higazi, J. R. Potts, D. C. Lowe, S. E. Radford and A. E. Ashcroft, *J. Am. Soc. Mass Spectrom.*, 2017, **28**, 1855-1862.
37. J. Y. Han, T. S. Choi, E. E. Heo, M. K. Son and H. I. Kim, *Mass Spectrom. Rev.*, 2019, **(in press)**.
38. A. D. Rolland and J. S. Prell, *Trac-Trends Anal. Chem.*, 2019, **116**, 282-291.
39. S. D. Pringle, K. Giles, J. L. Wildgoose, J. P. Williams, S. E. Slade, K. Thalassinos, R. H. Bateman, M. T. Bowers and J. H. Scrivens, *Int. J. Mass Spectrom.*, 2007, **261**, 1-12.
40. J. C. May, C. R. Goodwin, N. M. Lareau, K. L. Leaptrot, C. B. Morris, R. T. Kurulugama, A. Mordehai, C. Klein, W. Barry, E. Darland, G. Overney, K. Imatani, G. C. Stafford, J. C. Fjeldsted and J. A. McLean, *Anal. Chem.*, 2014, **86**, 2107-2116.
41. F. Fernandez-Lima, D. A. Kaplan, J. Suetering and M. A. Park, *Int. J. Mass Spectrom.*, 2011, **14**, 93-98.
42. S. A. Ewing, M. T. Donor, J. W. Wilson and J. S. Prell, *J. Am. Soc. Mass Spectrom.*, 2017, **28**, 587-596.
43. A. T. Iavarone and E. R. Williams, *J. Am. Chem. Soc.*, 2003, **125**, 2319-2327.
44. S. H. Lomeli, S. Yin, R. R. O. Loo and J. A. Loo, *J. Am. Soc. Mass Spectrom.*, 2009, **20**, 593-596.
45. C. A. Teo and W. A. Donald, *Anal. Chem.*, 2014, **86**, 4455-4462.
46. X. Han, M. Jin, K. Breuker and F. W. McLafferty, *Science*, 2006, **314**, 109-112.
47. N. Siuti and N. L. Kelleher, *Nat. Methods*, 2007, **4**, 817-821.
48. J. J. Coon, *Anal. Chem.*, 2009, **81**, 3208-3215.
49. R. A. Zubarev, A. R. Zubarev and M. M. Savitski, *J. Am. Soc. Mass Spectrom.*, 2008, **19**, 753-761.
50. J. B. Shaw, W. Li, D. D. Holden, Y. Zhang, J. Griep-Raming, R. T. Fellers, B. P. Early, P. M. Thomas, N. L. Kelleher and J. S. Brodbelt, *J. Am. Chem. Soc.*, 2013, **135**, 12646-12651.
51. S. R. Harvey, J. T. Seffernick, R. S. Quintyn, Y. Song, Y. Ju, J. Yan, A. N. Sahasrabuddhe, A. Norris, M. W. Zhou, E. J. Behrman, S. Lindert and V. H. Wysocki, *Proc. Natl. Acad. Sci. U. S. A.*, 2019, **116**, 8143-8148.
52. F. Lermyte, Y. O. Tsybin, P. B. O'Connor and J. A. Loo, *J. Am. Soc. Mass Spectrom.*, 2019, **30**, 1149-1157.
53. S. Consta, *J. Mol. Struct. (Theochem)*, 2002, **591**, 131-140.
54. S. Consta, M. I. Oh, M. Sharawy and A. Malevanets, *J. Phys. Chem. A*, 2018, **122**, 5239-5250.
55. V. Znamenskiy, I. Marginean and A. Vertes, *J. Phys. Chem. A*, 2003, **107**, 7406-7412.
56. S. S. Iyengar, T. J. F. Day and G. A. Voth, *Int. J. Mass Spectrom.*, 2005, **241**, 197-204.
57. C. Caleman and D. van der Spoel, *Phys. Chem. Chem. Phys.*, 2007, **9**, 5105-5111.
58. H. Higashi, T. Tokumi, C. J. Hogan, H. Suda, T. Seto and Y. Otani, *Phys. Chem. Chem. Phys.*, 2015, **17**, 15746-15755.

59. M. Porrini, F. Rosu, C. Rabin, L. Darre, H. Gomez, M. Orozco and V. Gabelica, *ACS Central Sci.*, 2017, **3**, 454–461.
60. D. Kim, N. Wagner, K. Wooding, D. E. Clemmer and D. H. Russell, *J. Am. Chem. Soc.*, 2017, **139**, 2981-2988.
61. S. G. Kondalaji, M. Khakinejad and S. J. Valentine, *J. Am. Soc. Mass Spectrom.*, 2018, **29**, 1665-1677.
62. R. Beveridge, L. G. Migas, R. K. Das, R. V. Pappu, R. W. Kriwacki and P. E. Barran, *J. Am. Chem. Soc.*, 2019, **141**, 4908-4918.
63. L. Konermann, H. Metwally, R. G. McAllister and V. Popa, *Methods*, 2018, **144**, 104-112.
64. A. Patriksson, E. Marklund and D. van der Spoel, *Biochemistry*, 2007, **46**, 933-945.
65. C. D. Daub and N. M. Cann, *Anal. Chem.*, 2011, **83**, 8372-8376.
66. J. L. P. Benesch, B. T. Ruotolo, D. A. Simmons and C. V. Robinson, *Chem. Rev.*, 2007, **107**, 3544-3567.
67. R. Juraschek, T. Dulcks and M. Karas, *J. Am. Soc. Mass Spectrom.*, 1999, **10**, 300-308.
68. I. Marginean, J. S. Page, A. V. Tolmachev, K. Q. Tang and R. D. Smith, *Anal. Chem.*, 2010, **82**, 9344-9349.
69. Y. Sun, S. Vahidi, M. A. Sowole and L. Konermann, *J. Am. Soc. Mass Spectrom.*, 2016, **27**, 31-40.
70. A. Gomez and K. Tang, *Phys. Fluids*, 1994, **6**, 404-414.
71. X. Wu, R. D. Oleschuk and N. M. Cann, *Analyst*, 2012, **137**, 4150-4161.
72. M. Samalikova and R. Grandori, *J. Am. Chem. Soc.*, 2003, **125**, 13352-13353.
73. R. L. Grimm and J. L. Beauchamp, *J. Phys. Chem. A*, 2010, **114**, 1411-1419.
74. R. Wang and R. Zenobi, *J. Am. Soc. Mass Spectrom.*, 2010, **21**, 378-385.
75. S. Zhou and K. D. Cook, *Anal. Chem.*, 2000, **72**, 963-969.
76. U. H. Verkerk and P. Kebarle, *J. Am. Soc. Mass Spectrom.*, 2005, **16**, 1325-1341.
77. Z. Z. Zhang, C. J. Pulliam, T. Flick and R. G. Cooks, *Anal. Chem.*, 2018, **90**, 3856-3862.
78. W. H. Wu, D. X. Zhang, K. X. Chen, P. Zhou, M. J. Zhao, L. Qiao and B. Su, *Anal. Chem.*, 2018, **90**, 14395-14401.
79. A. F. M. Gavriilidou, B. Gulbakan and R. Zenobi, *Anal. Chem.*, 2015, **87**, 10378-10384.
80. L. Konermann, *J. Am. Soc. Mass Spectrom.*, 2017, **28**, 1827-1835.
81. L. Rayleigh, *Philos. Mag.*, 1882, **14**, 184-186.
82. M. Chen, L. X. Zheng, B. Santra, H. Y. Ko, R. A. DiStasio, M. L. Klein, R. Car and X. F. Wu, *Nat. Chem.*, 2018, **10**, 413-419.
83. Y. X. Peng, J. M. J. Swanson, S. G. Kang, R. H. Zhou and G. A. Voth, *J. Phys. Chem. B*, 2015, **119**, 9212-9218.
84. S. Cukierman, *Biochim. Biophys. Acta*, 2006, **1757**, 876-885.
85. H. Metwally and L. Konermann, *Anal. Chem.*, 2018, **90**, 4126-4134.
86. S. Warnke, G. von Helden and K. Pagel, *J. Am. Chem. Soc.*, 2013, **135**, 1177-1180.
87. J. G. Bonner, N. G. Hendricks and R. R. Julian, *J. Am. Soc. Mass Spectrom.*, 2016, **27**, 1661-1669.
88. Y. Chen and M. T. Rodgers, *J. Am. Chem. Soc.*, 2012, **134**, 5863-5875.
89. I. G. Loscertales and J. F. de la Mora, *J. Chem. Phys.*, 1995, **103**, 5041-5060.
90. P. Nemes, I. Marginean and A. Vertes, *Anal. Chem.*, 2007, **79**, 3105-3116.
91. C. J. Hogan, J. A. Carroll, H. W. Rohrs, P. Biswas and M. L. Gross, *Anal. Chem.*, 2009, **81**, 369-377.
92. S. J. Allen, A. M. Schwartz and M. F. Bush, *Anal. Chem.*, 2013, **85**, 12055−12061.

93. E. Grifoni, G. Piccini and M. Parrinello, *Proc. Natl. Acad. Sci. U. S. A.*, 2019, **116**, 4054-4057.
94. M. Chen, H. Y. Ko, R. C. Remsing, M. F. C. Andrade, B. Santra, Z. R. Sun, A. Selloni, R. Car, M. L. Klein, J. P. Perdew and X. F. Wu, *Proc. Natl. Acad. Sci. U. S. A.*, 2017, **114**, 10846-10851.
95. D. Marx, M. E. Tuckerman, J. Hutter and M. Parrinello, *Nature*, 1999, **397**, 601-604.
96. K. B. Shelimov and M. F. Jarrold, *J. Am. Chem. Soc.*, 1997, **119**, 2987-2994.
97. M. T. Donor, S. A. Ewing, M. A. Zenaidee, W. A. Donald and J. S. Prell, *Anal. Chem.*, 2017, **89**, 5107-5114.
98. S. H. Lomeli, I. X. Peng, S. Yin, R. R. Ogorzalek Loo and J. A. Loo, *J. Am. Soc. Mass Spectrom.*, 2010, **21**, 127-131.
99. H. J. Sterling, M. P. Daly, G. K. Feld, K. L. Thoren, A. F. Kintzer, B. A. Krantz and E. R. Williams, *J. Am. Soc. Mass Spectrom.*, 2010, **21**, 1762-1774.
100. A. Kharlamova, B. M. Prentice, T.-Y. Huang and S. A. McLuckey, *Anal. Chem.*, 2010, **82**, 7422-7429.
101. R. Maurus, C. M. Overall, R. Bogumil, Y. Luo, A. G. Mauk, M. Smith and G. D. Brayer, *Biochim. Biophys. Acta*, 1997, **1341**, 1-13.
102. D. Eliezer, J. Yao, H. J. Dyson and P. E. Wright, *Nat. Struct. Biol.*, 1998, **5**, 148-155.
103. J. C. Kendrew, G. Bodo, H. M. Dintzis, R. G. Parrish, H. Wyckoff and D. C. Phillips, *Nature*, 1958, **181**, 662-666.
104. M. Fändrich, M. A. Fletcher and C. M. Dobson, *Nature*, 2001, **410**, 165-166.
105. F. M. Hughson, P. E. Wright and R. L. Baldwin, *Science*, 1990, **249**, 1544-1548.
106. P. A. Jennings and P. E. Wright, *Science*, 1993, **262**, 892-896.
107. I. Peters, H. Metwally and L. Konermann, *Anal. Chem.*, 2019, **91**, 6943-6952.
108. Wang, H., G. Yong, S. L. Brown, H. E. Lee, M. A. Zenaidee, C. T. Supuran and W. A. Donald, *Anal. Chim. Acta*, 2018, **1003**, 1-9.
109. P. D. Schnier, D. S. Gross and E. R. Williams, *J. Am. Soc. Mass Spectrom.*, 1995, **6**, 1086-1097.
110. M. A. Kelly, M. M. Vestling, C. C. Fenselau and P. B. Smith, *Org. Mass Spectrom.*, 1992, **27**, 1143-1147.
111. G. Wang and R. B. Cole, *Org. Mass Spectrom.*, 1994, **29**, 419-427.
112. T. Rob and D. J. Wilson, *J. Am. Soc. Mass Spectrom.*, 2009, **20**, 124-130.
113. M. J. Abraham, T. Murtola, R. Schulz, S. Páll, J. C. Smith, B. Hess and E. Lindahl, *SoftwareX*, 2015, **1–2**, 19-25.
114. R. G. McAllister, H. Metwally, Y. Sun and L. Konermann, *J. Am. Chem. Soc.*, 2015, **137**, 12667-12676.
115. H. Metwally, Q. Duez and L. Konermann, *Anal. Chem.*, 2018, **90**, 10069-10077.
116. F. J. de la Mora, *Anal. Chim. Acta*, 2000, **406**, 93-104.
117. I. A. Kaltashov and A. Mohimen, *Anal. Chem.*, 2005, **77**, 5370-5379.
118. N. G. Hendricks and R. R. Julian, *Analyst*, 2016, **141**, 4534-4540.
119. T. Wyttenbach and M. T. Bowers, *J. Phys. Chem. B*, 2011, **115**, 12266-12275.
120. D. E. Clemmer, D. H. Russell and E. R. Williams, *Accounts Chem. Res.*, 2017, **50**, 556-560.
121. E. Jurneczko and P. E. Barran, *Analyst*, 2011, **136**, 20-28.
122. J. T. S. Hopper and N. J. Oldham, *J. Am. Soc. Mass Spectrom.*, 2009, **20**, 1851-1858.
123. M. F. Bush, Z. Hall, K. Giles, J. Hoyes, C. V. Robinson and B. T. Ruotolo, *Anal. Chem.*, 2010, **82**, 9667-9565.

124. H. Metwally, R. G. McAllister, V. Popa and L. Konermann, *Anal. Chem.*, 2016, **88**, 5345-5354.
125. P. D. Compton, L. Zamdborg, P. M. Thomas and N. L. Kelleher, *Anal. Chem.*, 2011, **83**, 6868-6874.
126. A. G. Marshall, C. L. Hendrickson and G. S. Jackson, *Mass Spectrom. Rev.*, 1998, **17**, 1-35.
127. A. R. Zubarev and A. Makarov, *Anal. Chem.*, 2013, **85**, 5288-5296.
128. C. J. Hogan, R. R. Ogorzalek Loo, J. A. Loo and J. F. de la Mora, *Phys. Chem. Chem. Phys.*, 2010, **12**, 13476-13483.
129. Z. Hall, A. Politis, M. F. Bush, L. J. Smith and C. V. Robinson, *J. Am. Chem. Soc.*, 2012, **134**, 3429-3438.
130. C. M. Fisher, A. Kharlamova and S. A. McLuckey, *Anal. Chem.*, 2014, **86**, 4581-4588.
131. K. Chingin, N. Xu and H. Chen, *J. Am. Soc. Mass Spectrom.*, 2014, **25**, 928-934.
132. M. Zhou, S. Dagan and V. H. Wysocki, *Analyst*, 2013, **138**, 1353-1362.
133. C. N. Ferguson, S. A. Benchaar, Z. X. Miao, J. A. Loo and H. Chen, *Anal. Chem.*, 2011, **83**, 6468-6473.
134. R. R. Ogorzalek Loo, R. Lakshmanan and J. A. Loo, *J. Am. Soc. Mass Spectrom.*, 2014, **25**, 1675-1693.
135. M. Nshanian, R. Lakshmanan, H. Chen, R. R. Ogorzalek Loo and J. A. Loo, *Int. J. Mass Spectrom.*, 2018, **427**, 157–164.
136. K. A. Douglass and A. R. Venter, *J. Am. Soc. Mass Spectrom.*, 2012, **23**, 489-497.
137. M. Samalikova and R. Grandori, *J. Mass Spectrom.*, 2005, **40**, 503-510.
138. Y. Yao, M. R. Richards, E. N. Kitova and J. S. Klassen, *J. Am. Soc. Mass Spectrom.*, 2016, **27**, 498-506.
139. Z. Hall and C. V. Robinson, *J. Am. Soc. Mass Spectrom.*, 2012, **23**, 1161-1168.
140. H. J. Sterling, A. F. Kintzer, G. K. Feld, C. A. Cassou, B. A. Krantz and E. R. Williams, *J. Am. Soc. Mass Spectrom.*, 2012, **23**, 191-200.
141. J. B. Hedges, S. Vahidi, X. Yue and L. Konermann, *Anal. Chem.*, 2013, **85**, 6469-6476.
142. R. K. Boyd and Á. Somogyi, *J. Am. Soc. Mass Spectrom.*, 2010, **21**, 1275-1278.
143. A. R. Dongré, J. L. Jones, Á. Somogyi and V. H. Wysocki, *J. Am. Chem. Soc.*, 1996, **118**, 8365-8374.
144. J. Y. Li, W. P. Lyu, G. Rossetti, A. Konijnenberg, A. Natalello, E. Ippoliti, M. Orozco, F. Sobott, R. Grandori and P. Carloni, *J. Phys. Chem. Lett.*, 2017, **8**, 1105-1112.
145. S. Mehmood, T. M. Allison and C. V. Robinson, *Annu. Rev. Phys. Chem.*, 2015, **66**, 453-474.
146. R. Beveridge, A. S. Phillips, L. Denbigh, H. M. Saleem, C. E. MacPhee and P. E. Barran, *Proteomics*, 2015, **15**, 2872-2883.
147. B. L. Schwartz, J. E. Bruce, G. A. Anderson, S. A. Hofstadler, A. L. Rockwood, R. D. Smith, A. Chilkoti and P. S. Stayton, *J. Am. Soc. Mass Spectrom.*, 1995, **6**, 459-465.
148. N. Felitsyn, E. N. Kitova and J. S. Klassen, *Anal. Chem.*, 2001, **73**, 4647-4661.
149. J. L. P. Benesch, *J. Am. Soc. Mass Spectrom.*, 2009, **20**, 341-348.
150. S. K. Fegan and M. Thachuk, *J. Chem. Theory Comput.*, 2013, **9**, 2531-2539.
151. S. Consta and J. K. Chung, *J. Phys. Chem. B*, 2011, **115**, 10447-10455.
152. Q. Duez, H. Metwally and L. Konermann, *Anal. Chem.*, 2018, **90**, 9912-9920.
153. M. F. Ke, H. Zhang, J. H. Ding, X. C. Xiong, F. L. Li, K. Chingin, W. Kou, A. Y. Liu, T. G. Zhu, X. Fang and H. W. Chen, *Anal. Chem.*, 2019, **91**, 3215-3220.

154. M. A. Zenaidee, M. G. Leeming, F. T. Zhang, T. T. Funston and W. A. Donald, *Angew. Chem.-Int. Edit.*, 2017, **56**, 8522-8526.
155. B. A. Thomson, *J. Am. Soc. Mass Spectrom.*, 1997, **8**, 1053-1058.
156. K. J. Laszlo, E. B. Munger and M. F. Bush, *J. Am. Chem. Soc.*, 2016, **138**, 9581-9588.
157. K. B. Shelimov, D. E. Clemmer, R. R. Hudgins and M. F. Jarrold, *J. Am. Chem. Soc.*, 1997, **119**, 2240-2248.
158. S. Yin and J. A. Loo, *Int. J. Mass Spectrom.*, 2011, **300**, 118-122.
159. S. A. McLuckey, G. J. Van Berkel and G. L. Glish, *J. Am. Chem. Soc.*, 1990, **112**, 5668-5670.
160. S. Trimpin, I. Lu, S. Rauschenbach, K. Hoang, B. Wang, N. D. Chubatyi, W.-J. Zhang, E. D. Inutan, M. Pophristic, A. Sidorenko and C. N. McEwen, *J. Am. Soc. Mass Spectrom.*, 2018, **29**, 304-315.

Figure Captions

Figure 1. MD simulation data, illustrating various charge loss events of aqueous ESI droplets containing Na^+ (dark blue). (A) IEM ejection of a small Na^+/water cluster.[152] (B) IEM ejection of a Na^+/crown ether complex;, crown ether molecules are depicted in yellow/red.[85] (C) Formation of a small offspring droplet carrying one Na^+.[115] (D) Formation of a small offspring droplet carrying two Na^+.[152] Red lines in C/D indicate where the water filament is about to rupture. Droplet radii in A-D are between 4 and 5.5 nm. Droplets in panels A/D contain a synthetic polymer (green), droplets in panels B/C contain a protein (magenta and cyan). (E) Number of water molecules and Na^+ during evaporative droplet shrinkage. (F) Droplet charge z_D relative to the Rayleigh charge z_R. The droplet evolution proceeds along z_D = *constant* lines, depicted in grey.[152] Downward transitions arise from charge loss events. Modified with permission from refs.[85, 152] Copyright 2018, American Chemical Society.

Figure 2. Four types of protein ESI experimental conditions, illustrated for myoglobin (Mb). We distinguish native and denaturing ESI, each of which can be conducted without supercharging ("regular") and with supercharging. Experimental spectra are shown along the top. The corresponding proposed ESI mechanisms are depicted below in cartoon representation. (A) Native ESI of holo-Mb in neutral aqueous solution. (B) Native supercharging ESI of holo-Mb in neutral aqueous solution with 1% sulfolane. The inset shows the structure of sulfolane. (C) Denaturing ESI of apo-Mb in acidic aqueous solution. (D) Denatured supercharging ESI of apo-Mb in acidic aqueous solution with 1% sulfolane. Some holo ("h") and apo ("a") Mb charge states are indicated. Modified with permission from refs.[85, 107] Copyright 2018, 2019, American Chemical Society.

Figure 3. Snapshots of MD trajectories, depicting the formation of gaseous Mb ion from Rayleigh-charged ESI nanodroplets. Panels A-D refer to the experimental conditions of Figure 2A-D. (A) Native ESI of holo-Mb in water, forming a native-like 9+ ion. (B) Native supercharging ESI of holo-Mb in water/sulfolane, generating holo-Mb 16+. (C) Denaturing ESI of acid-unfolded apo-Mb, producing a stretched-out 22+ gaseous ion. (D) Denatured supercharging of acid-unfolded apo-Mb in water/sulfolane, culminating in a highly extended 27+ ion. Panels A/B follow the CRM, while C/D exhibit CEM behavior. Some Na^+ IEM ejection events are highlighted. Coloring is as follows: protein, purple; water oxygen, red; Na^+, blue; sulfolane, green. Modified with permission from refs.[85, 107] Copyright 2018, 2019, American Chemical Society.

Figure 4. Analogy between (A) the chain ejection model (CEM), and (B) the collision-induced dissociation of a noncovalent protein complex. Excess H^+ are indicated as "+". In (A), an unfolded protein is ejected from an ESI droplet. The protruding tail undergoes charge equilibration with the droplet via H^+ migration. The protein leaves as a highly charged unfolded ion. In (B), protein subunits are depicted as spheres. One subunit (red) undergoes unfolding, and the protruding tail accumulates charge due to H^+ migration from the residual complex. The subunit leaves as a highly charged unfolded ion. Modified from ref.[6] Copyright 2013, American Chemical Society.

Figure 5. MD snapshots of CEM events, depicting apo-Mb 27+ chains that are about to separate from an ESI droplet. (A) Water droplet. (B) Water/sulfolane droplet. Close-ups highlight some charged residues (cyan) and their solvation by residual water (panel A) and water/sulfolane (panel B). Solvation in (B) is much more extensive, providing greater stabilization of protonated sites in the presence of sulfolane. Modified from ref.[107] Copyright 2019, American Chemical Society.

Figure 1

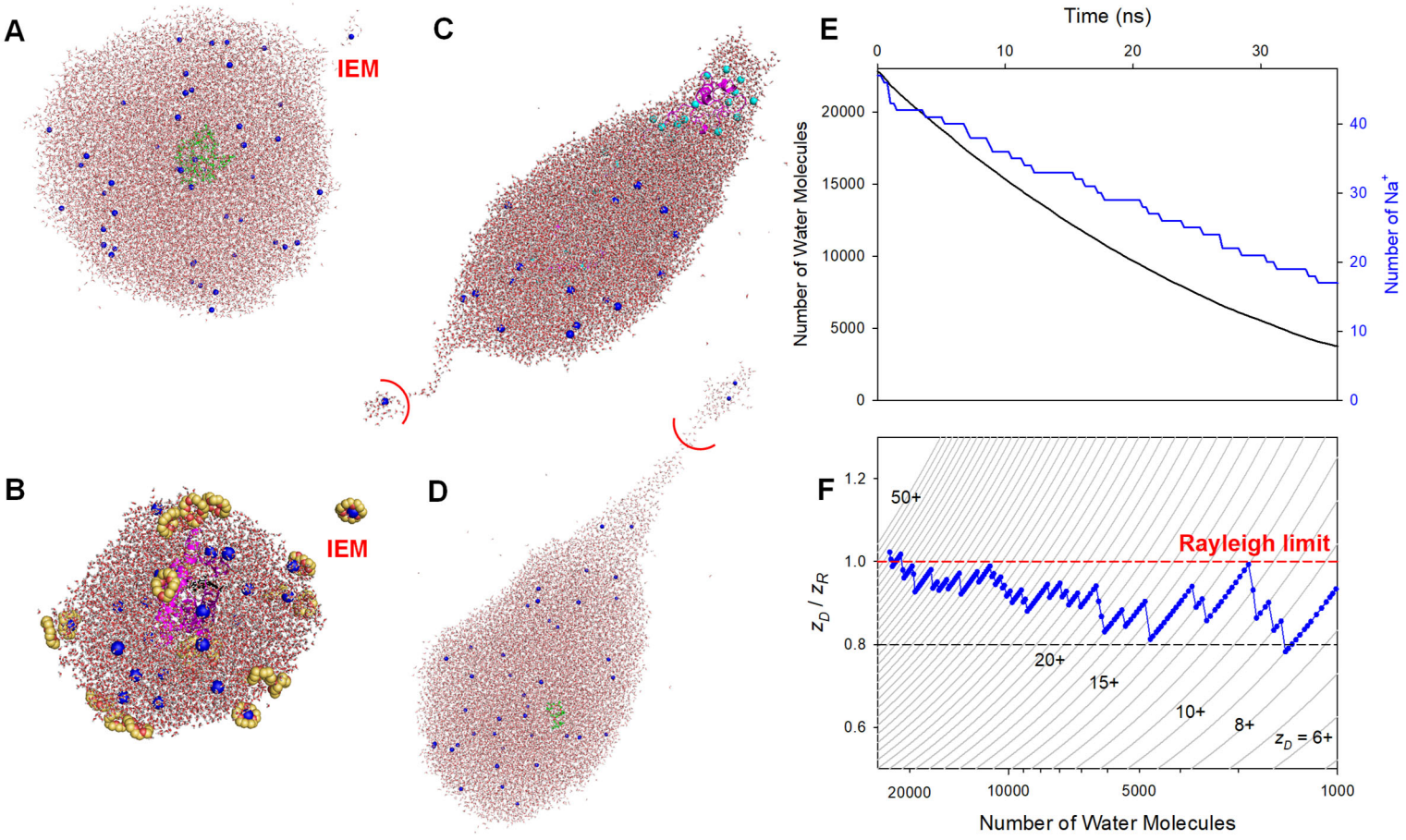
A
IEM
B
IEM
C
D
E
Time (ns)
0
10
20
30
Number of Water Molecules
20000
15000
10000
5000
0
Number of Na+
40
30
20
10
0
F
50+
Rayleigh limit
20+
15+
10+
8+
zD = 6+
zD / zR
1.2
1.0
0.8
0.6
20000
10000
5000
1000
Number of Water Molecules

Figure 2

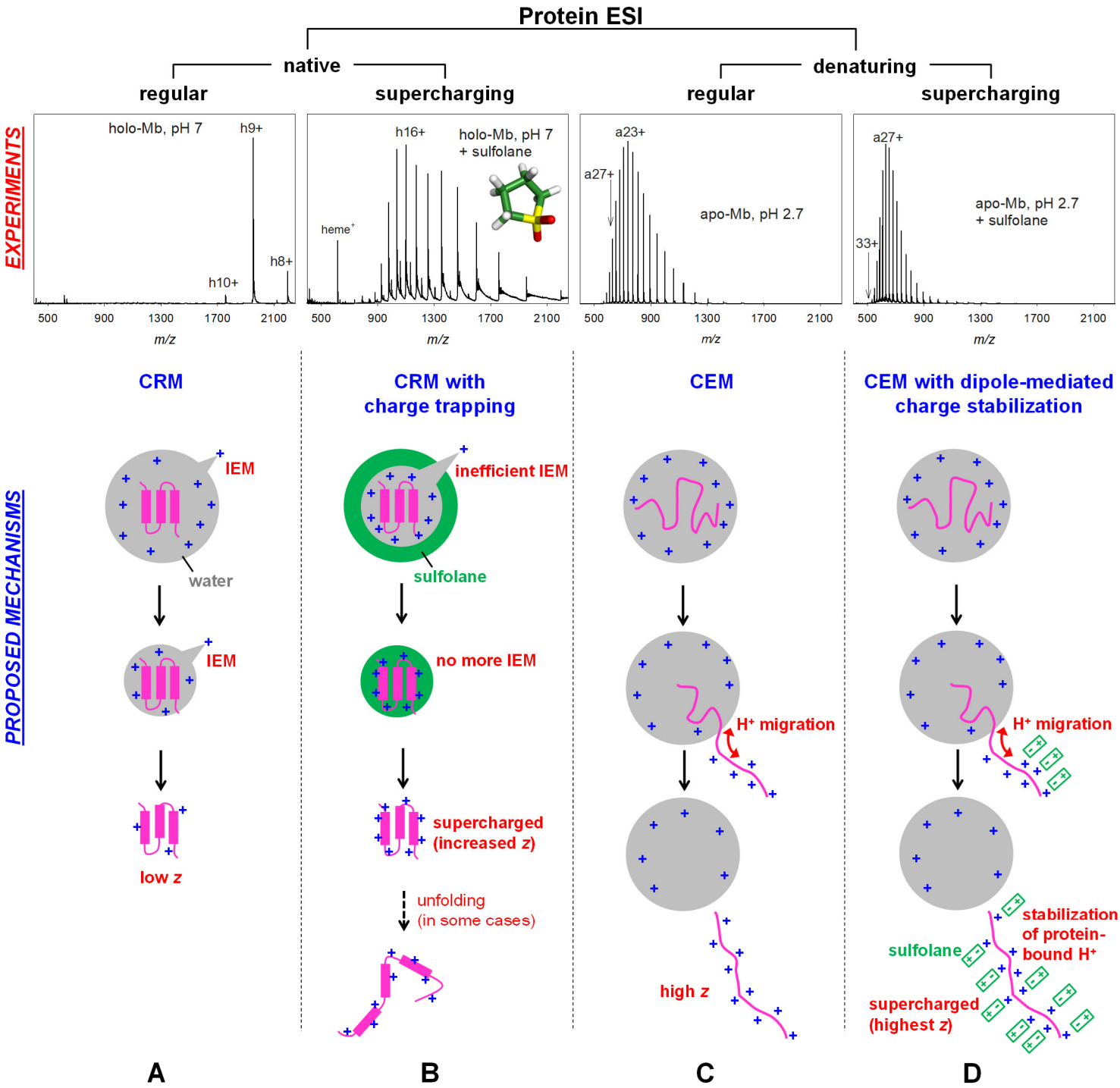
Protein ESI
native
denaturing
regular
supercharging
regular
supercharging
EXPERIMENTS
holo-Mb, pH 7
h9+
h10+
h8+
h16+
holo-Mb, pH 7
+ sulfolane
heme+
a23+
a27+
apo-Mb, pH 2.7
a27+
apo-Mb, pH 2.7
+ sulfolane
33+
500
900
1300
1700
2100
m/z
PROPOSED MECHANISMS
CRM
CRM with
charge trapping
CEM
CEM with dipole-mediated
charge stabilization
IEM
water
IEM
low z
inefficient IEM
sulfolane
no more IEM
supercharged
(increased z)
unfolding
(in some cases)
H+ migration
high z
H+ migration
stabilization
of protein-
bound H+
sulfolane
supercharged
(highest z)
A
B
C
D

Figure 3

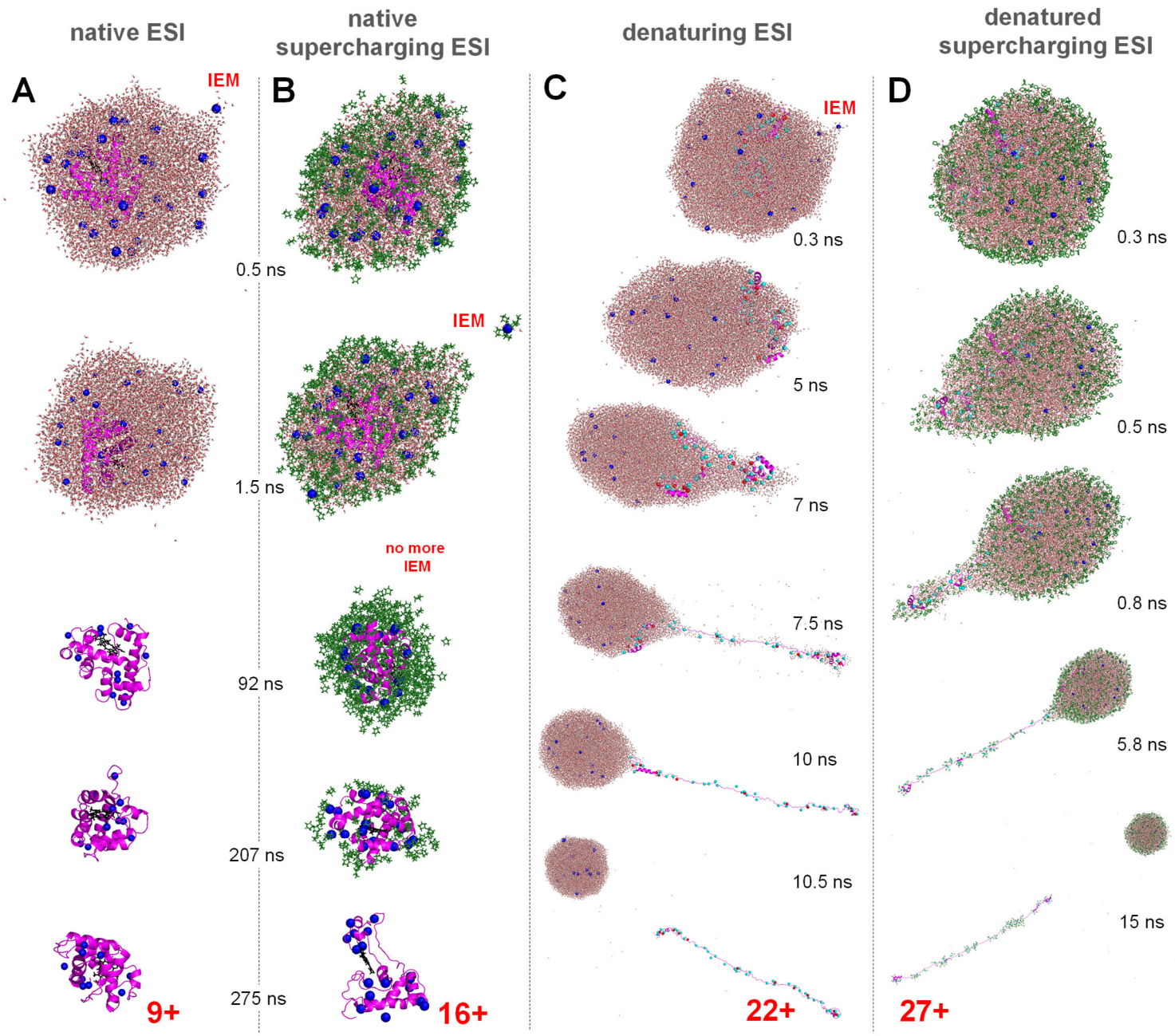
native ESI
native supercharging ESI
denaturing ESI
denatured supercharging ESI
A
B
C
D
IEM
0.5 ns
IEM
1.5 ns
no more IEM
92 ns
207 ns
275 ns
9+
16+
IEM
0.3 ns
5 ns
7 ns
7.5 ns
10 ns
10.5 ns
22+
0.3 ns
0.5 ns
0.8 ns
5.8 ns
15 ns
27+

Figure 4

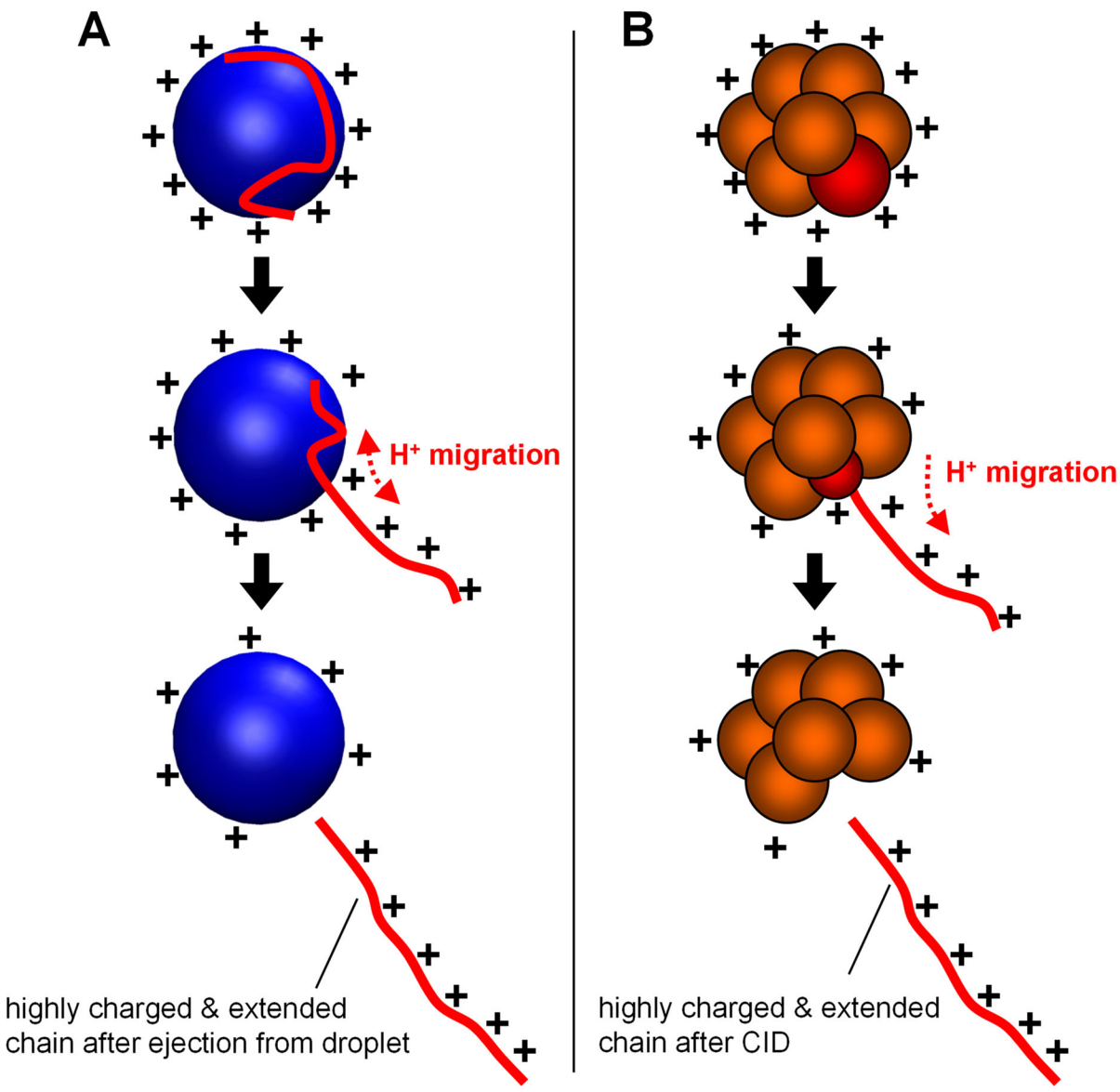
A
B
H+ migration
H+ migration
highly charged & extended
chain after ejection from droplet
highly charged & extended
chain after CID

Figure 5

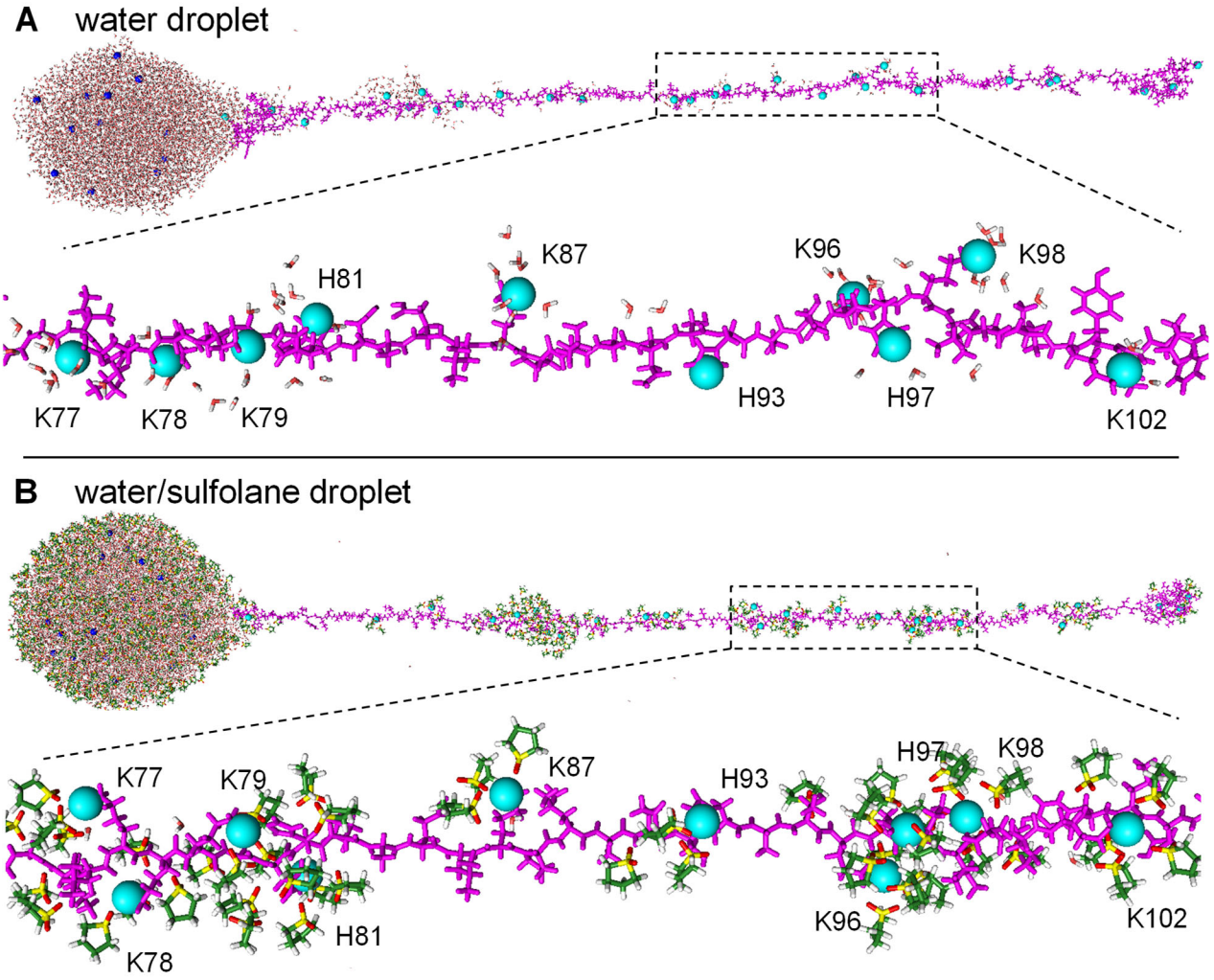
A water droplet
K77
K78
K79
H81
K87
H93
K96
H97
K98
K102
B water/sulfolane droplet
K77
K79
K78
H81
K87
H93
H97
K98
K96
K102

TOC Figure

[please resize TOC graphic to journal specifications by dragging one of the corner points]

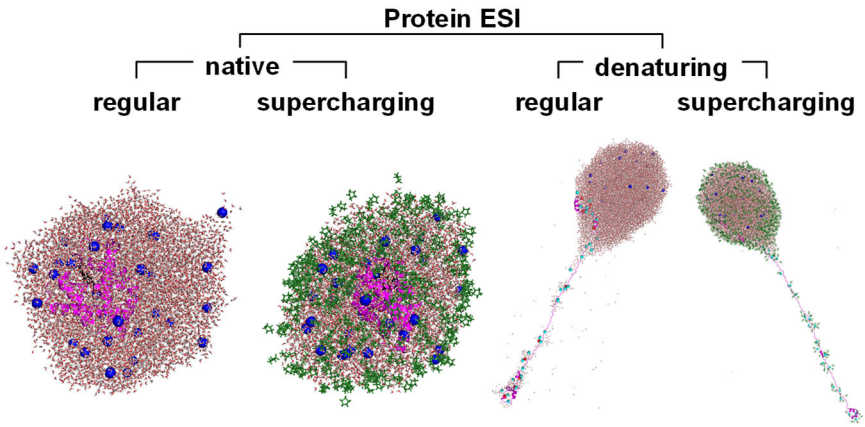

TOC text: “Molecular dynamics simulations have uncovered mechanistic details of the protein ESI process under various experimental conditions”